ACS NANO
Cite This: ACS Nano 2018, 12, 576−584
www.acsnano.org

ARTICLE

Room-Temperature Magnetic Switching of the Electric Polarization in Ferroelectric Nanopillars

Shashi Poddar,* Pedro de Sa, Ronggang Cai, Laurent Delannay, Bernard Nysten, Luc Piraux, and Alain M. Jonas*

Institute of Condensed Matter & Nanosciences, Bio & Soft Matter Université Catholique de Louvain, Louvain-la-Neuve, BE 1348, Belgium

Supporting Information

ABSTRACT: **Magnetoelectric layers with a strong coupling between ferroelectricity and ferromagnetism offer attractive opportunities for the design of new device architectures such as dual-channel memory and multiresponsive sensors and actuators. However, materials in which a magnetic field can switch an electric polarization are extremely rare, work most often only at very low temperatures, and/or comprise complex materials difficult to integrate. Here, we show that magnetostriction and flexoelectricity can be harnessed to strongly couple electric polarization and magnetism in a regularly nanopatterned magnetic metal/ferroelectric polymer layer, to the point that full reversal of the electric polarization can occur at room temperature by the sole application of a magnetic field. Experiments supported by finite element simulations demonstrate that magnetostriction produces large strain gradients at the base of the ferroelectric nanopillars in the magnetoelectric hybrid layer, translating by flexoelectricity into equivalent electric fields larger than the coercive field of the ferroelectric polymer. Our study shows that flexoelectricity can be advantageously used to create a very strong magnetoelectric coupling in a nanopatterned hybrid layer.**

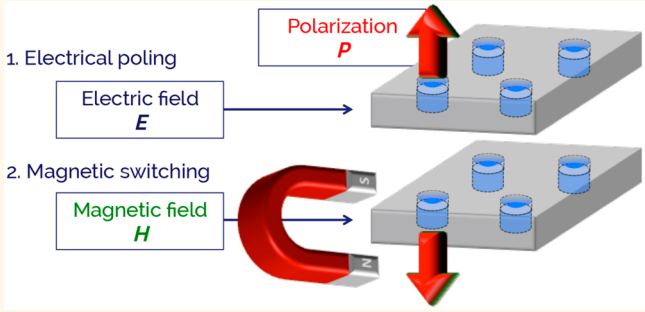

KEYWORDS: *multiferroics, nanoimprinting, magnetoelectric effect, piezoresponse force microscopy, ferroelectric polymer, flexoelectricity, magnetostriction*

Multiferroic systems involve the coexistence and coupling of two or more ferroic orders,[1] with applications in robust dual-channel memory storage and multiresponsive sensors and actuators. The coupling of ferroelectricity with ferromagnetism is particularly interesting for data storage applications, as it might enable reading/writing magnetic data by electrical means or *vice versa*.[2] Therefore, extensive efforts have been devoted to developing new materials wherein the magnetization can be controlled by an electric field or the electric polarization by a magnetic field. However, room-temperature permanent switching of an electrical polarization by a magnetic field *alone* in a patterned storage medium has so far been elusive. Here, we design a regularly patterned layer in which the electric polarization can be permanently flipped at room temperature by the sole application of a magnetic field, and demonstrate that this coupling is mediated by flexoelectricity as opposed to the more classically used piezoelectricity.

There have been widespread efforts in synthesizing single-phase multiferroic materials,[3−5] but certain desirable characteristics for the manifestation of both ferroelectricity and ferromagnetism tend to be conflicting in nature.[6] Possible alternate routes such as metal organic frameworks,[7] magnetic spirals,[8,9] and charge-ordering magnets[10] have also been investigated with moderate success, because they often suffer from charge instabilities reducing the net spontaneous polarization and mostly need cryogenic temperatures for magnetoelectric coupling. However, rapid progress has been made in multiphase systems such as composites,[11] laminates,[12] and epitaxial heterostructures,[13] in which indirect magnetoelectric coupling occurs between ferroelectric and ferromagnetic regions through the mediation of magnetostriction and piezoelectricity.[14] Multicomponent metal/organic multilayers[15,16] and nanostructures of 1−3 connected architecture[17] have shown room-temperature tuning of the electric polarization by a magnetic field, but permanent switching of the

Received: October 18, 2017
Accepted: January 3, 2018
Published: January 3, 2018

DOI: 10.1021/acsnano.7b07389
ACS Nano 2018, 12, 576−584

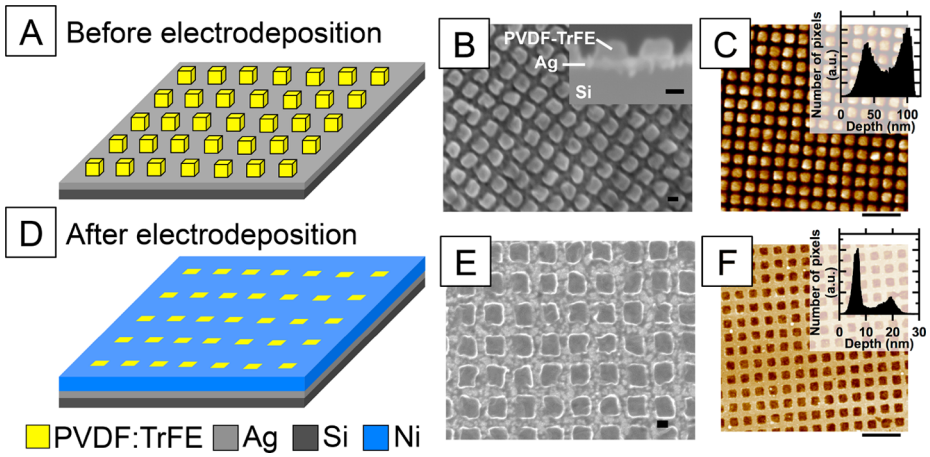

Figure 1. Structure of the samples before (A–C) and after (D–F) electrodeposition of the Ni matrix. A and D are schematic structures, B and E are SEM images, and C and F are the AFM tapping mode topography images. The inset in B is a cross-sectional cut of the sample (scale bar 50 nm), and the insets in panels C and F are histograms of pixel heights. Scale bars in images are 100 nm for SEM and 800 nm for AFM, respectively.

electric polarization of patterned domains by a magnetic field alone has never been demonstrated at room temperature. Even in single-phase multiferroics, room-temperature magnetic field switching of the ferroelectric polarization was very rarely reported, as in thin crystalline lamellae of solid solution mixtures of lead zirconium titanate and lead iron tantalate (PZTFT).[18] However, in the authors' own words, the switching process was "largely irreversible and stochastic in nature" with "sporadic and unpredictable large changes in domain states", illustrating the difficulties associated with magnetically switching a ferroelectric state.

We recently demonstrated that,[19] in a 1–3 connected multiferroic hybrid layer consisting of ferromagnetic nickel nanopillars regularly embedded in a ferroelectric polymer matrix, the ferroelectric polarization could be switched using magnetic fields up to 0.5 T aided by an electric field that is about 5 times smaller than the actual switching fields. The substrate-clamped Ni pillars expand in plane and contract out of plane upon application of a magnetic field, creating a significant magnetostrictive strain. This strain transfers to the polymer and couples to the ferroelectric order parameter, resulting in chain segmental motion and dipole reversal in the ferroelectric medium. The small electric field prevents the dipoles from relaxing back to the original polarization states. The effect was tentatively attributed to several factors, one being the flexoelectric effect.

Flexoelectricity is a universal phenomenon that induces an electric polarization in a dielectric medium due to a strain gradient, in contrast with piezoelectricity, where the stress creates the change of polarization.[20,21] Cross[22] and co-workers used a square truncated pyramidal[23,24] geometry to study flexoelectricity, since the mismatch of top and bottom areas produces a strain gradient under compressive loading, yielding measurable bound charges on the electrodes.[25] We reasoned that, since the flexoelectric effect involves a gradient of strain and is thus inversely proportional to the length scale of a device, the nanopatterning of a ferroelectric ultrathin film would amplify the flexoelectric effect. Furthermore, taking a cue from Cross' square truncated pyramidal geometry, we fabricated soft ferroelectric polymer nanopillars embedded in a hard electrodeposited ferromagnetic Ni matrix, the reverse geometry of the one we used before.[19] Owing to its negative magnetostriction coefficient, the Ni grid will expand in the plane and be compressed out of the plane of the film when applying an out-of-plane magnetic field;[26] due to the physical clamping of Ni on the substrate, the strain will be increasing from bottom to top and couple to the adjoining soft ferroelectric nanopillars, which will suffer maximal compression at their top free end, effectively leading to a vertical gradient of strain along the pillar length. This design is thus optimal for enhancing flexoelectric effects under a magnetic field, leading to the possible switching of polarization by a magnetic field alone. That flexoelectricity might be used to switch prepoled ferroelectric domains is testified by a pioneering work by Lu[27] *et al.*, in which strain gradients were locally built with an atomic force microscopy (AFM) tip applying force on epitaxial $BaTiO_3$ thin films. In the present work, however, the flexoelectric-induced fields will be generated by a magnetic field through the creation of a magnetostrictive strain.

RESULTS AND DISCUSSION

Whereas in almost all prior works including our own[19] on multiferroic composite systems of 1–3 connectivity[28] the device geometry comprises ferromagnetic pillars embedded in a ferroelectric matrix, here we developed the reverse architecture of ferroelectric square pillars embedded in a ferromagnetic matrix in order to maximize the flexoelectric effect as opposed to the more usual piezoelectric effect. The ferroelectric material is the copolymer of vinylidene fluoride (VDF) with trifluoroethylene (TrFE) in the weight ratio 75:25. The copolymer PVDF:TrFE is a flexible material that can be efficiently molded in regular fully confined high-density arrays of crystalline nanopillars by nanoimprint lithography.[29] S. Poddar *et al.* have studied the flexoelectric effect in the family of VDF-based copolymers[30] and obtained a moderate flexoelectric coefficient of 0.191 μC/m in the ferroelectric phase.[31,32] The ferromagnetic material used in this work is electrodeposited nickel with a large magnetostriction coefficient at saturation[33,26] (λ) of (4 to 7) $\times$ 10^{-5}, which forms a polycrystalline mesh confining the ferroelectric pillars clamped to the substrate (Figure 1D).

Regular periodic arrays of ferroelectric square pillars were obtained by nanoimprint lithography over large areas (Figure 1B,C), with no residual film connecting the pillars (inset of Figure 1B). The average pillar height from the histogram of

DOI: 10.1021/acsnano.7b07389
ACS Nano 2018, 12, 576–584

pixel height is 62 ± 2 nm. After optimization of the nanoimprinting process, nickel was electrochemically deposited to fill the regions surrounding the ferroelectric nanostructures. This is a critical step, which needs a calibration of the final deposited charge to avoid under- or overfilling of the interstitial spaces (Supporting Information, Figure S3). The optimal charge in our particular case was 20 mC. Scanning electron microscopy (SEM) images after electrochemical deposition of nickel show a high contrast along the spaces surrounding the ferroelectric nanopillars (Figure 1E). Tapping mode AFM (Figure 1F) provided an average difference of height between the top of the Ni grid and the top of the PVDF:TrFE pillars of 10 ± 1 nm. The magnetic hysteresis loops for the nanohybrid multiferroic layer were measured using alternating gradient magnetometry at room temperature for both in-plane and out-of-plane orientations of the sample (Figure S4), revealing that the Ni grid grown by electroplating has an easy axis in the plane of the substrate and a hard axis perpendicular to the plane with a saturation field beyond 6 kOe, as expected from magnetostatic arguments.[34]

The ferroelectric properties of the nanopillars were first characterized by piezoresponse force microscopy (PFM) before and after electrodeposition of the ferromagnetic nickel matrix (Supporting Information, Figure S5). The PFM phase and amplitude hysteresis loops were then acquired on individual ferroelectric nanopillars embedded in the Ni matrix while applying a gradually increased dc magnetic field oriented in the out-of-plane direction with respect to the planar substrate. A strong coupling between electric polarization and magnetic field was detected, with a narrowing of hysteresis loops upon application of the magnetic field. Figure 2A and B show the PFM phase and amplitude hysteresis for two contact frequencies, either at the resonance frequency (363 kHz, B) or off-resonance (100 kHz, A). In both cases, the PFM phase loops span 180°, confirming complete domain switching, and the hysteresis loop width decreases with magnetic field with a stronger effect seen on the positive bias side. The average coercive field was computed from the hysteresis loop half-width and is plotted in Figure 2C. The coercive field first decreases strongly with increasing magnetic field, by up to a factor of 4 when measured at resonance; for higher magnetic fields, the effect tends to saturate. The PFM amplitude is one order of magnitude larger for on- compared to off- resonance due the increased quality factor at/near contact resonance.[35]

The magnetic switching of the electric polarization was then studied by measuring local PFM phase and amplitude while applying steps of magnetic field of increasing strength. The initial contact mode topography, PFM amplitude, and PFM phase signals were mapped for a 4 μm^2 area of the hybrid multiferroic layer in Figure 3A–C before any electrical poling and magnetic field treatment. Three selected ferroelectric nanopillars were then poled with a −6 V bias applied through the PFM tip for 5 s, thereby switching the local ferroelectric domains upward (Supporting Information, Figure S6). Next, the dc voltage was zeroed, and the magnetic field was repeatedly turned on and off (1 s rise time) while recording the PFM signals over one of the prepoled pillars. This experiment was performed for magnetic fields of 4.1, 6, and 7.2 kOe while measuring over pillars 1, 2, and 3 in Figure 3, respectively. For pillars 1 and 2 (Figure 3G,H), the local PFM phase difference between the magnetic on- and off-states is close to 180° and the amplitude signal also increases in the magnetic on-state, revealing downward flipping of the polarization upon application of the magnetic field. However, this flipping is not stable since the PFM signal comes back to its initial value in the magnetic off-state. In contrast, when the magnetic field was increased further to 7.2 kOe (spot 3, Figure 3I), the local PFM phase signal did not switch back to the initial phase value even when the magnetic field was turned off, indicating permanent switching of the polarization. The amplitude signal also stayed at the high magnetic "on" value when the magnetic field was turned off, confirming that the local ferroelectric domains are now permanently switched in the direction opposite the initial polarization. Importantly, this behavior is not observed when the ferroelectric nanopillars are prepoled downward using a +6 V bias. In this case, the downwardly poled regions do not show clear and permanent phase changes upon application of a magnetic field (Supporting Information Figure S7), indicating that magnetic switching occurs only for upwardly poled regions.

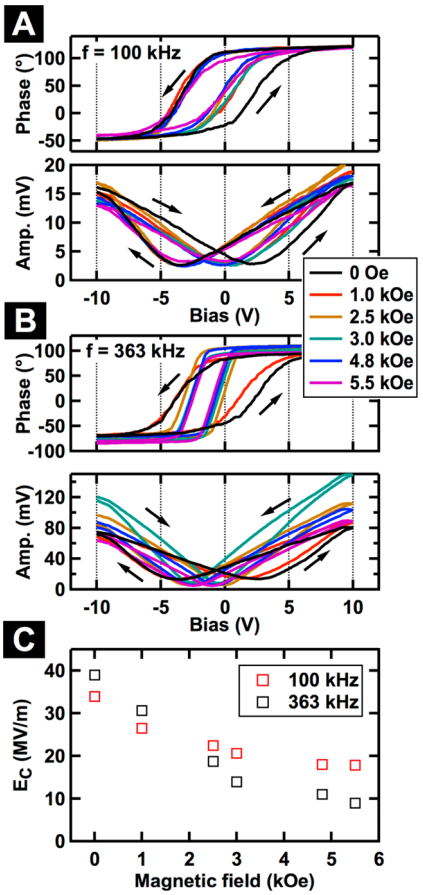

Figure 2. Dependence of local PFM hysteresis loops on the out-of-plane magnetic field: (A) off-resonance (100 kHz), (B) on-resonance (363 kHz), (C) variation of the average electric coercive field with magnetic field.

After acquiring the local PFM signals on the three prepoled ferroelectric nanopillars, another spot marked 4 was locally upwardly poled with −6 V for 5 s for reference, and the sample was imaged again (Figure 3D–F). The poled spot 4 shows a bright PFM contrast relative to its surroundings. In contrast, spot 3 where the PFM signal was monitored for 7.2 kOe shows a majority darker contrast in the center with a narrow brighter annular region indicative of a switching of the underlying ferroelectric domains in the center of the spot. Spots 1 and 2 also indicate permanent switching at some locations, since

DOI: 10.1021/acsnano.7b07389
ACS Nano 2018, 12, 576–584

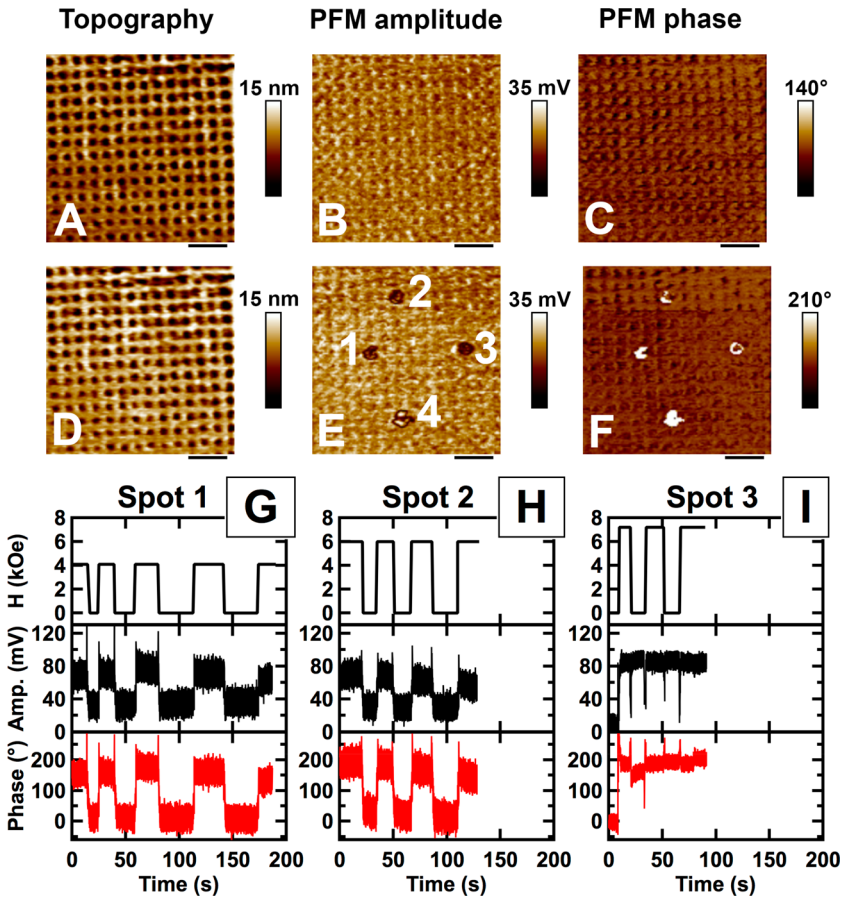

Figure 3. Switching of locally prepoled ferroelectric nanopillars by application of a magnetic field. (A, B, C) PFM topography, amplitude, and phase of the as-fabricated region. (D, E, F) PFM mapping after electric field poling and magnetic field treatment for spots 1 (4.1 kOe), 2 (6 kOe), and 3 (7.2 kOe) and after only electric field poling for spot 4. (G, H, I) Variation of the local PFM phase and amplitude upon application of steps of magnetic field at spots 1−3. The scale bars for the PFM images are 830 nm.

these spots also felt the 7.2 kOe magnetic field applied during the local PFM measurement of spot 3 (the magnetic field being applied to the whole sample).

In the previous experiments, the magnetic field was applied while the AFM tip was on the prepoled spot. The surface contact force is estimated to be only 50 nN directly below the tip, which should not be enough to cause tip-induced switching. However, to rule out any parasitic tip effect, an alternate experiment was conducted, wherein four individual ferroelectric nanopillars were poled by a −6 V dc bias (in the yellow frame of Figure 4), and a 7.2 kOe magnetic field was applied *after tip removal*. PFM images were acquired before poling (Figure 4A−C), after poling (Figure 4D−F), and after the application of the magnetic field (Figure 4G−I), showing either complete erasure or strong shrinkage of the poled dots by the application of the magnetic field. Incomplete domain shrinkage is most probably due to domain pinning defects either resulting from electrodeposition or arising from the presence of crystal grain boundaries.

Permanent reversal of the polarization by a magnetic field at room temperature in a patterned hybrid structure, in the absence of any other aiding field, has not been reported so far and provides new opportunities for sensing devices and memories. The origin of the phenomenon is the change of polarization arising from the mechanical deformation of the polymer nanopillars, resulting from the magnetostrictive deformation of the magnetic matrix. The nickel grid matrix has a negative magnetostriction coefficient, leading on average to out-of-plane contraction and in-plane expansion in the presence of an out-of-plane magnetic field. Clamping on the substrate implies that the in-plane deformation increases from the bottom to the top of the film. Because the Young's modulus of Ni (200 GPa)[26] is *ca.* 2 orders of magnitude larger than that of PVDF:TrFE (2.5 GPa),[36] the polymer nanopillars do not constrain much the deformation of the Ni grid. Polymer nanopillars are hence laterally compressed, with the compressive strain gradually increasing along their height. This results in deformed nanopillars of a slightly pyramidal shape. The presence of a strain gradient in the vertical direction can induce a change of polarization of the polymer either through the piezoelectric effect, for which polarization is linearly proportional to the stress, or through the flexoelectric effect, for which polarization is proportional to the gradient of strain, or through both.

An estimation of the relative importance of each effect can be obtained with a simple model in which the in-plane compressive strain in the nanopillars is approximated to be a linear function of the pillar height coordinate x_3, with no deformation at the contact with the substrate and free deformation at the film top surface: $\varepsilon_{11}(x_3) = \beta\lambda x_3/h$, where h is the film thickness, $\lambda \approx -40 \times 10^{-6}$ is the average saturation magnetostriction coefficient of the magnetic matrix,[37,38] and β is a geometrical factor on the order of 1 whose exact value depends on the precise architecture and on the Poisson ratio of

DOI: 10.1021/acsnano.7b07389
ACS Nano 2018, 12, 576−584

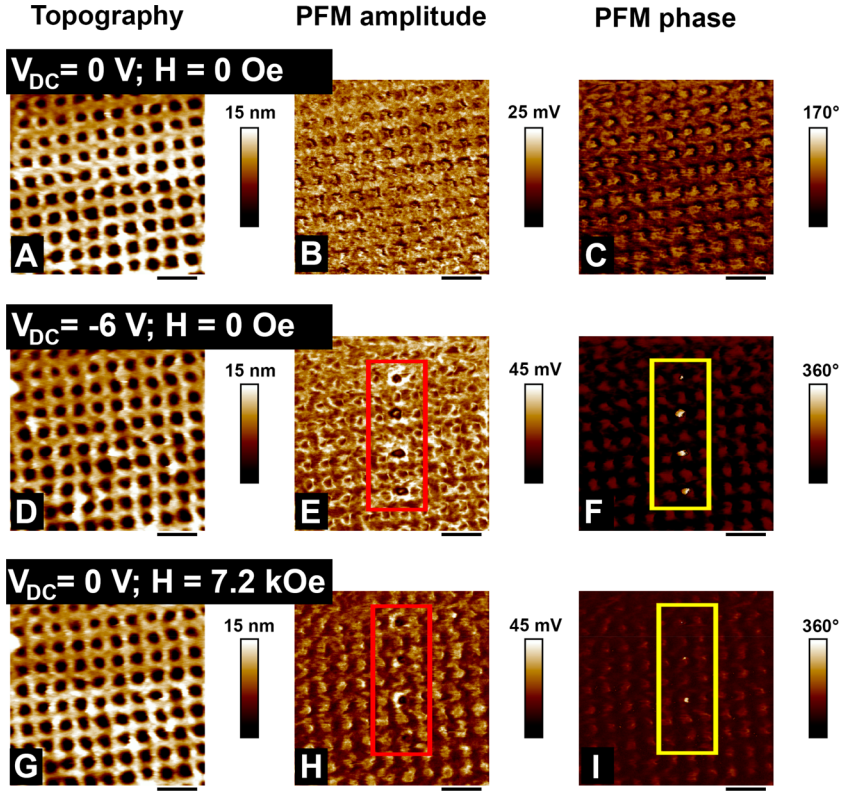

Figure 4. Magnetic switching of locally prepoled ferroelectric nanopillars in the absence of any PFM tip. (A, B, C) PFM topography, amplitude, and phase of the as-fabricated region. (D, E, F) PFM mapping after electric field poling of four selected spots. (G, H, I) PFM mapping of the same region after application of a magnetic field of 7.2 kOe, showing the switching or strong shrinkage of prepoled spots. The scale bar is 600 nm.

the magnetic nanogrid. The maximum change of polarization in the vertical direction (index 3) due to piezoelectricity is therefore $\Delta P_{3,\text{piezo}} \approx \beta d_{31} E \lambda$, with $E \approx 2.5 \times 10^9$ Pa being the Young's modulus of the polymer and $d_{31} \approx 20 \times 10^{-12}$ C/N being the proper piezoelectric coefficient.[36] The change of polarization arising from flexoelectricity is $\Delta P_{3,\text{flexo}} \approx f(\mathrm{d}\varepsilon_{11}/\mathrm{d}x_3) \approx \beta f \lambda / h$, with $f \approx 191 \times 10^{-9}$ C/m being the flexoelectric coefficient of the copolymer.[30] The ratio between the flexoelectric and piezoelectric contributions to the change of polarization is thus independent of the magnetostriction coefficient and reads $\Delta P_{3,\text{flexo}}/\Delta P_{3,\text{piezo}} = \alpha h^{-1}$ with $\alpha = f/(d_{31}E) \approx 3.8$ μm. Hence, flexoelectricity becomes the dominant factor for films of thickness in the submicrometer range as used in the present study, for which piezoelectricity can be completely neglected.

In this simple model, the change of polarization due to flexoelectricity for $h = 65$ nm and $\lambda = -40 \times 10^{-6}$ is $\Delta P_{3,\text{flexo}} \approx -117\beta$ μC/m^2, where the negative sign indicates a reduction (respectively increase) of the amplitude of an upward- (respectively downward-) pointing polarization. This change of polarization is equivalent to that caused by the application of a downward-pointing external electric field of amplitude $\Delta P_{3,\text{flexo}}/(k-1)\varepsilon_0 \approx -\beta$ MV/m, where $k \approx 15$ is the dielectric constant[39] and ε_0 is the dielectric permittivity of a vacuum. Thus, applying the out-of-plane magnetic field is equivalent to applying a positive electric potential to the top of the nanopillars, the bottom electrode being grounded. Therefore, a region prepoled with a negative bias by the PFM tip will be switched in this event in the opposite state, provided the electric field generated by the strain gradient is equal to or greater than the coercive field of the nanoconfined ferroelectric copolymer. The lack of permanent magnetic switching observed when the starting polarization is downward-pointing (Figure S7 in the Supporting Information) confirms that the equivalent electric field is then pointing in the same direction as the polarization, which obviously prevents polarization reversal.

Assuming the geometrical factor β to be on the order of unity, the strain-gradient electric fields mediated by the magnetostriction setting in the nickel nanogrid for this simplistic model is on the order of 1 MV/m. However, the magnetostriction coefficient of the nickel in the nanogrid is not known with precision, and the hypothesis of linearity of the lateral strain is a very rough approximation (as will be shown shortly). Hence, considering that the nanoimprinting process results in decreasing coercive fields (*ca.* 8 MV/m) due to increased crystalline perfection and improved preferential orientation,[40,41] the switching of an upward-pointing polarization by the flexoelectricity-generated equivalent electric field appears to be a plausible assumption.

For a more realistic estimate of the strain gradient-induced electric field in the hybrid multiferroic layer, finite element analysis (FEA) was employed. The specific parameters used for the FEA simulations are detailed in the Methods section. The negative magnetostriction in the nickel matrix was mimicked by a thermal stimulus causing anisotropic and volume-preserving fictitious thermal strains. The film was fully clamped at the bottom electrode, slip was impeded at the metal/polymer interface, and periodic boundary conditions were applied along the lateral edges of the finite element mesh. The vertical displacement field U_3 in one-quarter of a repeat unit of the film

DOI: 10.1021/acsnano.7b07389
ACS Nano 2018, 12, 576–584

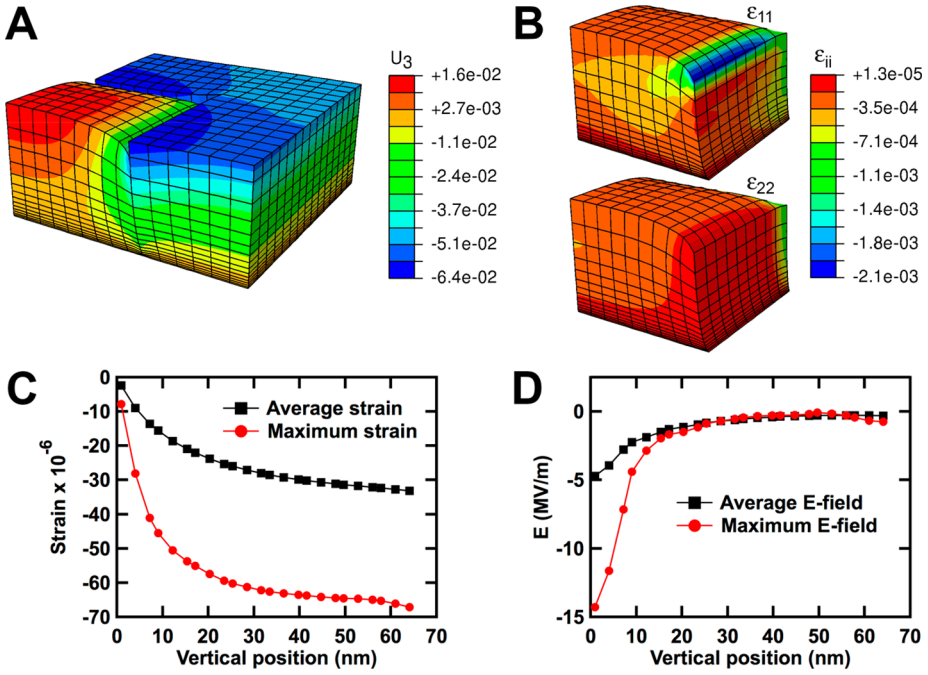

Figure 5. (A) Vertical displacement field in the pillars and matrix normalized by the magnetostrictive strain, (B) principal in-plane strains in the pillars normalized by the magnetostrictive strain, (C) average and maximum strains in the pillars along the vertical position, and (D) average and maximum strain-gradient-generated electric fields along the vertical position of the pillar. To help visualization, the deformations of the mesh are amplified by a factor of 10 in A and B.

is shown in Figure 5A, together with the deformation of the mesh; the Ni matrix contracts (negative U_3) and the pillars are forced to follow along the interface with the matrix. However, the pillars expand (positive U_3) along their central axis as a reaction (Poisson effect) to the in-plane compression. The in-plane principal strains are negative in most of the nanopillar volume (Figure 5B), except at the contact with the undeformable bottom electrode. Their average as well as maximum values are plotted *versus* vertical position in Figure 5C. The through-thickness gradient is nonuniform, unlike the simple model assumed earlier, with a strain gradient concentrating over the first 20 nm close to the substrate.

The strain gradient calculated from the finite element analysis is then multiplied by the effective value of the flexoelectric coefficient coefficient $F = f/(k - 1)\varepsilon_0$ of the copolymer reported elsewhere,[30] which results in an equivalent flexoelectricity-generated electric field profile varying as shown in Figure 5D. In this figure, we have plotted both the average flexoelectricity-generated equivalent electric field and the maximum electric field as a function of the vertical position along the ferroelectric pillar. Since local ferroelectric domain nucleation will start at the location of the maximum electric field, one must consider the maximum electric fields and not only the average values. Once the nucleation event sets in, the switching of the domain can then be propagated laterally for lower values of electric field.[42,43] The strain-gradient-generated electric field is maximum at the clamped end with a value close to −15 MV/m as shown in Figure 5D, which is large enough for ferroelectric switching in an array of fully nanoconfined PVDF:TrFE pillars. Indeed, coercive fields of *ca.* 8 MV/m have been reported before for such confined systems.[40] Figure 2A and B also show that magnetic fields high enough to saturate the magnetic moments of the nickel nanogrid lead to a decrease of the switching voltage to below 0 V. The nucleation of the ferroelectric domains starts at the bottom end of the pillars, from which it grows laterally by flipping the dipoles along a crystalline chain of the PVDF:TrFE and then propagates from chain to chain in the forward direction, eventually switching the negatively poled dots. The presence of structural defects might however hinder the forward domain propagation, leading to incomplete switching. This is corroborated by the observation of both complete and partial erasure of the negatively poled ferroelectric nanopillars when applying the saturation vertical magnetic field (Figure 4).

Because the maximal strain gradient controls the flexoelectric effect, it is important to understand the geometrical parameters controlling the size and location of the high-strain-gradient region. First, simulations performed for a series of pillar heights indicated that this region of maximal strain gradient is essentially independent of the pillar height. Second, since the FEA simulations can be scaled by any spatial factor f_s in the three spatial directions without any change of the results, it follows that the size of the high-strain-gradient region directly scales with the repeat period of the pattern; therefore, the magnitude of the gradient increases for smaller repeat periods. This conclusion is also supported by performing an analysis in analogy with the case of the thermal expansion of cylindrical posts clamped at one end on a surface, for which a quasi-analytical solution exists.[44] For this case also, a high strain region exists in direct vicinity of the clamped end, over a region of size varying in proportion to the radius of the post. This confirms that magnetic switching of the polarization would be improved by further reducing the lateral size of the pattern. In contrast, reducing the height of the layer will not change the initiation of the switching; it might however make the propagation of the switching easier, once initiated.

DOI: 10.1021/acsnano.7b07389
ACS Nano 2018, 12, 576−584

CONCLUSION

In summary, we have shown by piezoelectric force microscopy the complete polarization reversal of ferroelectric domains by the application of a magnetic field alone at room temperature. This was achieved by designing a nanohybrid device architecture consisting of ferroelectric nanopillars of the soft PVDF:TrFE copolymer in a nickel magnetic matrix. The magnetostrictive strain in the magnetic matrix couples to the ferroelectric nanopillars, building up a significant strain gradient at the base of the clamped pillars. The strain gradient in turn produces an equivalent electric field by the flexoelectric effect, which is of the same magnitude as the field required to switch a negatively poled ferroelectric domain of the copolymer. In order to support these experimental findings, a finite element simulation was used to model the strain in the nanohybrid system and estimate from it the induced electric fields.

In the present study in which a magnetic metal with a negative magnetostriction was used, the clamping condition only allows the reversal with a vertical magnetic field of negatively poled ferroelectric domains (upward-pointing polarization). However, the use of magnetic materials of opposite magnetostriction coefficient would provide us with an opportunity to design layers in which a downward-pointing polarization could be magnetically switched. More importantly, our study demonstrates that strong coupling of magnetic and electric orders can happen in hybrid polymer-based nanostructures thanks to the flexoelectric effect as opposed to the more usual piezoelectric effect. With more complex patterns and some ingenuity, the possibility to design bidirectional magnetically switchable multiferroic hybrid devices operating through flexoelectricity appears thus to be within our reach.

METHODS

Fabrication of the Hybrid Layers. Silicon wafers with 20 nm of electron-beam deposited silver were used as substrates. PVDF:TrFE (75:25 wt %, Solvay Specialty Polymers) was dissolved in DMSO (reagent grade, Sigma-Aldrich) to a concentration of 5% by weight; 250 μL was spin-coated at 3500 rpm and 2000 acceleration to obtain a thin film of 50 nm average thickness in the ferroelectric β-phase (Supporting Information Figure S1). The nanopillar array structure was fabricated in a class 1000 cleanroom environment by nanoimprinting (Obducat nanoimprinter, 60 bar, 130 °C, 30 min) with a perfluorosilanized hard silicon mold of 4 mm^2 effective template area, consisting of square holes of 200 nm side, 100 nm depth, and 300 nm periodicity (scheme in Figure S2). The surrounding nickel structure was deposited by electrochemical deposition with periodic pulses of −1.09 V for 10 ms and −0.7 V for 90 ms for a final deposition charge of 20 mC. The periodic potential was applied at room temperature to a 0.5 M $NiSO_4{\cdot}6H_2O$/0.4 M H_3BO_3 electrolytic solution through a dual-junction Ag/AgCl reference electrode and a Pt reference electrode attached to a PAR 263A potentiostat.

Characterization of the Layers. The topography of the nanoimprinted structures was studied with a Bruker Icon Dimension AFM in tapping mode using an AR5T-NCHR high aspect ratio tip (k = 42 N/m, f = 330 kHz, tip radius = 15 nm) commercially obtained from Nanosensors. SEM measurements were obtained with a JEOL 7600F. Ferroelectric properties were characterized by piezoelectric force microscopy (Bruker Icon Dimension) in the optimized vertical domain mode with a deflection set point less than 50 nN and a Pt/Ir-coated tip (Bruker SCM-PITV2, k = 2.8 N/m, f = 360 kHz, tip radius = 20 nm). Poling was performed by applying the proper voltage to the tip, the bottom electrode of the sample being grounded. The test ac signal was always 2.0 V in amplitude unless mentioned otherwise. The magnetic field up to 10 kOe in the out-of-plane direction was applied from the bottom using a Helmholtz coil obtained from Bouchnik SAS, France, equipped with a cooling circuit and integrated into the scanning probe system. The magnetic measurements were always performed with a custom-made nonmagnetic tip holder from Bruker Inc. Images were acquired with 512 pixels/line, except when in the presence of a magnetic field, for which 128 pixels/line were used to minimize aperiodic drifts resulting from the water cooling of the Helmholtz coil.

Finite Element Analysis Calculations. Predictions of strain heterogeneity were performed using the Abaqus finite element code. The two constitutive materials were assigned uniform and isotropic elastic properties. Magnetostriction was accounted for by prescribing a fictitious temperature change and by relying on a functionality of Abaqus that is typically used to model anisotropic thermal strains. Indeed, both magnetostriction and thermal strains occur at constant stress (unlike elastic strains). The induced "thermal" strains were here designed to be nil inside the ferroelectric pillars, whereas the magnetic nanogrids underwent a volume-preserving strain: If 3 is the index associated with the out-of-plane direction of the film, $\varepsilon_{11} = \varepsilon_{22} = -\varepsilon_{33}/2$ with ε_{ii} being the diagonal components of the strain tensor. Compatible deformation of the two constituents of the film was then achieved by superposing to the thermal strain a heterogeneous elastic strain field. The latter was computed by the finite element solver in such a way as to satisfy stress equilibrium and to avoid geometrical mismatch throughout the volume.

The periodicity of the microstructure was accounted for by applying "mirror" boundary conditions, *i.e.*, zero out-of-plane displacement of the nodes, along planar edges of the mesh which were aligned parallel to the channels and which were positioned at the midwidth of either a channel or a pillar. The interface with the substrate (bottom edge of the mesh) was considered infinitely stiff (zero nodal displacements in all directions), whereas the top edge of the mesh was a free surface (zero nodal forces). The finite element mesh was selectively refined near the substrate, where strain gradients are largest. Simulations were performed using second-order brick-shaped elements with 20 nodes (C3D20), and the total number of elements inside the mesh (confining a quarter of a periodic unit) was sufficiently large to reproduce accurately the strain gradients; that is, using a more refined mesh did not change the predictions.

Since magnetostriction induces infinitesimal strains, the elastic response was linear and the simulation involved a single time increment. In order to visualize the film deformation in Figure 5A, strains were amplified by a factor 10. The outcome of the simulation indicates that the principal strains are aligned close to the two (orthogonal) channel directions, with the exception of the corner edges of the pillars, where shear strains are significant. The gradient of elastic strains through the thickness of the film, which is at the origin of flexoelectricity, was estimated by computing the average principal strains and maximum strains at different depth inside the modeled pillar.

ASSOCIATED CONTENT

Supporting Information

The Supporting Information is available free of charge on the ACS Publications website at DOI: 10.1021/acsnano.7b07389.

X-ray diffraction of the spin-coated thin films of PVDF:TrFE, scheme of the nanoimprinting process, SEM images for calibrating the optimal final charge for Ni electrodeposition, magnetic anisotropy of the electrodeposited nickel grid, PFM characterization of the pure nanoimprinted ferroelectric arrays, magnetic-field-dependent PFM measurements for positively poled nanopillars (PDF)

AUTHOR INFORMATION

Corresponding Authors

*E-mail: shashi.poddar@uclouvain.be.
*E-mail: alain.jonas@uclouvain.be.

DOI: 10.1021/acsnano.7b07389
ACS Nano 2018, 12, 576−584

ORCID

Alain M. Jonas: 0000-0002-4083-0688

Notes

The authors declare no competing financial interest.

ACKNOWLEDGMENTS

Financial support was provided by the Belgian Science Policy (IAP P7/05), the Wallonia/Brussels Community (ARC 13/18-052), and the Belgian Fund for Scientific Research (FNRS).

REFERENCES

(1) Kimura, T.; Goto, T.; Shintani, H.; Ishizaka, K.; Arima, T.; Tokura, Y. Magnetic Control of Ferroelectric Polarization. *Nature* **2003**, *426*, 55−58.
(2) Eerenstein, W.; Mathur, N.; Scott, J. F. Multiferroic and Magnetoelectric Materials. *Nature* **2006**, *442*, 759−765.
(3) Lunkenheimer, P.; Müller, J.; Krohns, S.; Schrettle, F.; Loidl, A.; Hartmann, B.; Rommel, R.; de Souza, M.; Hotta, C.; Schlueter, J. A.; Lang, M. Multiferroicity in an Organic Charge-transfer Salt That Is Suggestive of Electric-Dipole-Driven Magnetism. *Nat. Mater.* **2012**, *11*, 755−758.
(4) Kagawa, F.; Horiuchi, S.; Tokunaga, M.; Fujioka, J.; Tokura, Y. Ferroelectricity in a One-Dimensional Organic Quantum Magnet. *Nat. Phys.* **2010**, *6*, 169−172.
(5) Qin, W.; Chen, X.; Li, H.; Gong, M.; Yuan, G.; Grossman, J. C.; Wuttig, M.; Ren, S. Room Temperature Multiferroicity of Charge Transfer Crystals. *ACS Nano* **2015**, *9*, 9373−9379.
(6) Hill, N. A. Why Are There so Few Magnetic Ferroelectrics? *J. Phys. Chem. B* **2000**, *104*, 6694−6709.
(7) Jain, P.; Ramachandran, V.; Clark, R. J.; Zhou, H. D.; Toby, B. H.; Dalal, N. S.; Kroto, H. W.; Cheetham, A. K. Multiferroic Behavior Associated with an Order−Disorder Hydrogen Bonding Transition in Metal−Organic Frameworks (MOFs) with the Perovskite ABX_3 Architecture. *J. Am. Chem. Soc.* **2009**, *131*, 13625−13627.
(8) Kenzelmann, M.; Harris, A. B.; Jonas, S.; Broholm, C.; Schefer, J.; Kim, S. B.; Zhang, C. L.; Cheong, S. W.; Vajk, O. P.; Lynn, J. W. Magnetic Inversion Symmetry Breaking and Ferroelectricity in $TbMnO_3$. *Phys. Rev. Lett.* **2005**, *95*, 087206.
(9) Cheong, S.-W.; Mostovoy, M. Multiferroics: a Magnetic Twist for Ferroelectricity. *Nat. Mater.* **2007**, *6*, 13−20.
(10) van den Brink, J.; Khomskii, D. I. Multiferroicity due to Charge Ordering. *J. Phys.: Condens. Matter* **2008**, *20*, 434217.
(11) Nan, C.-W.; Bichurin, M. I.; Dong, S.; Viehland, D.; Srinivasan, G. Multiferroic Magnetoelectric Composites: Historical Perspective, Status, and Future Directions. *J. Appl. Phys.* **2008**, *103*, 031101.
(12) Lin, Y.; Cai, N.; Zhai, J.; Liu, G.; Nan, C.-W. Giant Magnetoelectric Effect in Multiferroic Laminated Composites. *Phys. Rev. B: Condens. Matter Mater. Phys.* **2005**, *72*, 012405.
(13) Wang, J.; Neaton, J. B.; Zheng, H.; Nagarajan, V.; Ogale, S. B.; Liu, B.; Viehland, D.; Vaithyanathan, V.; Schlom, D. G.; Waghmare, U. V.; Spaldin, N. A.; Rabe, K. M.; Wuttig, M.; Ramesh, R. Epitaxial $BiFeO_3$ Multiferroic Thin Film Heterostructures. *Science* **2003**, *299*, 1719−1722.
(14) Spaldin, N. A.; Fiebig, M. Materials science. The Renaissance of Magnetoelectric Multiferroics. *Science* **2005**, *309*, 391−392.
(15) Mardana, A.; Ducharme, S.; Adenwalla, S. Ferroelectric Control of Magnetic Anisotropy. *Nano Lett.* **2011**, *11*, 3862−3867.
(16) Mardana, A.; Bai, M.; Baruth, A.; Ducharme, S.; Adenwalla, S. Magnetoelectric Effects in Ferromagnetic Cobalt/Ferroelectric Copolymer Multilayer Films. *Appl. Phys. Lett.* **2010**, *97*, 112904.
(17) Aimon, N. M.; Kim, D. H.; Sun, X.; Ross, C. A. Multiferroic Behavior of Templated $BiFeO_3$−$CoFe_2O_4$ Self-Assembled Nanocomposites. *ACS Appl. Mater. Interfaces* **2015**, *7*, 2263−2268.
(18) Evans, D. M.; Schilling, A.; Kumar, A.; Sanchez, D.; Ortega, N.; Arredondo, M.; Katiyar, R. S.; Gregg, J. M.; Scott, J. F. Magnetic Switching of Ferroelectric Domains at Room Temperature in Multiferroic PZTFT. *Nat. Commun.* **2013**, *4*, 1534.
(19) Cai, R.; Antohe, V. A.; Hu, Z.; Nysten, B.; Piraux, L.; Jonas, A. M. Multiferroic Nanopatterned Hybrid Material with Room-Temperature Magnetic Switching of the Electric Polarization. *Adv. Mater.* **2017**, *29*, 1604604.
(20) Tagantsev, A. K. Piezoelectricity and Flexoelectricity in Crystalline Dielectrics. *Phys. Rev. B: Condens. Matter Mater. Phys.* **1986**, *34*, 5883−5889.
(21) Zubko, P.; Catalan, G.; Tagantsev, A. K. Flexoelectric Effect in Solids. *Annu. Rev. Mater. Res.* **2013**, *43*, 387−421.
(22) Cross, L. E. Flexoelectric Effects: Charge Separation in Insulating Solids Subjected to Elastic Strain Gradients. *J. Mater. Sci.* **2006**, *41*, 53−63.
(23) Fousek, J.; Cross, L. E.; Litvin, D. B. Possible Piezoelectric Composites Based on the Flexoelectric Effect. *Mater. Lett.* **1999**, *39*, 287−291.
(24) Fu, J. Y.; Zhu, W.; Li, N.; Smith, N. B.; Eric Cross, L. Gradient Scaling Phenomenon in Microsize Flexoelectric Piezoelectric Composites. *Appl. Phys. Lett.* **2007**, *91*, 182910.
(25) Ma, W.; Cross, L. E. Flexoelectric Polarization of Barium Strontium Titanate in the Paraelectric State. *Appl. Phys. Lett.* **2002**, *81*, 3440−3442.
(26) Cullity, B. D.; Graham, C. D. *Introduction to Magnetic Materials*; Wiley: Hoboken, 2009.
(27) Lu, H.; Bark, C. W.; Esque de los Ojos, D.; Alcala, J.; Eom, C. B.; Catalan, G.; Gruverman, A. Mechanical Writing of Ferroelectric Polarization. *Science* **2012**, *336*, 59−61.
(28) Palneedi, H.; Annapureddy, V.; Priya, S.; Ryu, J. Status and Perspectives of Multiferroic Magnetoelectric Composite Materials and Applications. *Actuators* **2016**, *5*, 9.
(29) Hu, Z.; Tian, M.; Nysten, B.; Jonas, A. M. Regular arrays of Highly Ordered Ferroelectric Polymer Nanostructures for Non-Volatile Low-Voltage Memories. *Nat. Mater.* **2009**, *8*, 62−67.
(30) Poddar, S.; Ducharme, S. Measurement of the Flexoelectric Response in Ferroelectric and Relaxor Polymer Thin Films. *Appl. Phys. Lett.* **2013**, *103*, 202901.
(31) Poddar, S.; Ducharme, S. Temperature Dependence of Flexoelectric Response in Ferroelectric and Relaxor Polymer Thin Films. *J. Appl. Phys.* **2014**, *116*, 114105.
(32) Poddar, S.; Foreman, K.; Adenwalla, S.; Ducharme, S. Finite-Size Scaling of Flexoelectricity in Langmuir-Blodgett Polymer Thin Films. *Appl. Phys. Lett.* **2016**, *108*, 012908.
(33) Klokholm, E. The Measurement of Magnetostriction in Ferromagnetic Thin Films. *IEEE Trans. Magn.* **1976**, *12*, 819−821.
(34) Sellmyer, D. J.; Zheng, M.; Skomski, R. Magnetism of Fe, Co and Ni Nanowires in Self-Assembled Arrays. *J. Phys.: Condens. Matter* **2001**, *13*, R433.
(35) Gruverman, A.; Auciello, O.; Tokumoto, H. Imaging and Control of Domain Structures in Ferroelectric Thin Films via Scanning Force Microscopy. *Annu. Rev. Mater. Sci.* **1998**, *28*, 101−123.
(36) Nalwa, H. S. *Ferroelectric Polymers: Chemistry: Physics, and Applications*; Marcel Dekker: New York, 1995.
(37) Klokholm, E.; Aboaf, J. The Saturation Magnetostriction of Thin Polycrystalline Films of Iron, Cobalt, and Nickel. *J. Appl. Phys.* **1982**, *53*, 2661−2663.
(38) Chopra, I.; Sirohi, J. *Smart Structures Theory*; Cambridge University Press: New York, 2014.
(39) Furukawa, T. Ferroelectric Properties of Vinylidene Fluoride Copolymers. *Phase Transitions* **1989**, *18*, 143−211.
(40) Kassa, H. G.; Cai, R.; Marrani, A.; Nysten, B.; Hu, Z.; Jonas, A. M. Structure and Ferroelectric Properties of Nanoimprinted Poly(Vinylidene Fluoride-*ran*-Trifluoroethylene). *Macromolecules* **2013**, *46*, 8569−8579.
(41) Kassa, H. G.; Nougaret, L.; Cai, R.; Marrani, A.; Nysten, B.; Hu, Z.; Jonas, A. M. The Ferro- to Paraelectric Curie Transition of a Strongly Confined Ferroelectric Polymer. *Macromolecules* **2014**, *47*, 4711−4717.
(42) Ishibashi, Y.; Takagi, Y. Note on Ferroelectric Domain Switching. *J. Phys. Soc. Jpn.* **1971**, *31*, 506−510.

DOI: 10.1021/acsnano.7b07389
ACS Nano 2018, 12, 576−584

(43) Wu, Y.; Li, X.; Jonas, A. M.; Hu, Z. Two-Step Polarization Switching in Ferroelectric Polymers. *Phys. Rev. Lett.* **2015**, *115*, 267601.
(44) Janak, J. F. Thermal Expansion in a Constrained Elastic Cylinder. *IBM J. Res. Dev.* **1969**, *13*, 323−330.

DOI: 10.1021/acsnano.7b07389
ACS Nano 2018, 12, 576−584